

Thermodynamics

Chemical Programming of the Domain of Existence of Liquid Crystals

Thibault Dutronc,^[a] Emmanuel Terazzi,^{*[a]} Laure Guénée,^[b] Kerry-Lee Buchwalder,^[a] Sébastien Floquet,^[c] and Claude Piguet^{*[a]}

Abstract: This work illustrates how enthalpy and entropy changes responsible for successive phase transitions of cyanobiphenyl-based liquid crystals can be combined to give cohesive free energy densities. These new parameters are able to rationalize and quantify the demixing of the melting and clearing processes that occur in thermotropic liquid

crystals. Minor structural variations at the molecular level can be understood as pressure increments that alter either the melting or clearing temperatures in a predictable way. This assessment of microsegregation operating in amphiphilic molecules paves the way for the chemical programming of the domain of existence of liquid-crystalline phases.

Introduction

After more than a century of scientific interest in liquid crystals, the prediction and fine-tuning of mesomorphism, as well as the design of new liquid-crystalline materials, is still a vast and fascinating issue.^[1] Because most existing applications for information display are based on liquid-crystal mixtures,^[2] decisive advances in the design of pure compounds and control of their properties would have significant industrial repercussions. So far, guidelines for the preparation of new mesomorphic materials have come from extensive empirical observations and pattern recognitions. If characteristic factors, such as molecular shapes, interfacial curvatures, or intermolecular interactions, have been clearly identified and can be selectively worked upon, studied, or even predicted by analogy, there is no unified route for the design of liquid crystals.^[3] From a chemical point of view, the industrially relevant^[2] thermotropic mesophase corresponds to a liquid-crystalline phase thermally induced by the melting of the solid, but separated from the isotropic liquid by the clearing process. Classical theories based on entropically driven hard-rod models,^[4] or on statistical treatments of long-range enthalpic contributions to the attractive

intermolecular potentials operating between interacting molecules in liquid crystals,^[5] were able to explain the occurrence of order–disorder phase transitions involving nematic organizations, but gave few insights into the prediction of the associated transition temperatures. A more recent model considers the two nanospaces of the incompatible components of a binary A–B amphiphilic molecule, which can be related to the macroscopic segregation (demixing) of two liquids with molecular structures similar to the two segments A and B that form the amphiphile (see Figures 1 and 2, below, for molecular illustrations).^[6] Because the empirical Trouton's rule fixes a value of $\Delta S_{\text{vap}} = 85\text{--}88 \text{ J mol}^{-1} \text{ K}^{-1}$ for the entropy of vaporization of any liquid, its enthalpy of vaporization, ΔH_{vap} , is linearly related to its vaporization temperature, $T_{\text{vap}} = \Delta H_{\text{vap}} / \Delta S_{\text{vap}}$.^[7] Therefore, ΔH_{vap} has been exploited as a quantitative index to estimate the intermolecular cohesive energy densities, $\delta^2 = \Delta H_{\text{vap}} / V_{\text{mol}}$, within liquids (V_{mol} is the molar volume and δ is known as the Hildebrand solubility parameter).^[8] The difference, $\delta_A - \delta_B$, between the two segments A and B of the amphiphile thus reflects their incompatibility and decides whether nanoscale segregation could take place.^[6] This approach is analogous to that originally developed for the miscibility of block copolymers,^[9] an analogy noted 40 years ago,^[10] which has found a renewal of interest^[11] for understanding the formation of mesophases in unconventional liquid-crystalline molecules.^[12] The basic concept considers the free energy of mixing for the formation of polymer blends, which includes standard entropy of mixing that arises from regular solution theory, together with an extra enthalpic contribution to monitor intermolecular interactions.^[9] The Flory and Huggins theory, in terms of solubility parameters, shows that the latter interaction factor depends on $(\delta_A - \delta_B)^2$ weighted by the thermal energy.^[6,12] Quantitative applications to mesogenic calamitic cyanobiphenyls,^[9a] cubic-phase-forming liquid-crystalline molecules,^[9c] and polycatenar pentaerythritol derivatives^[11b] successfully rationalized phase segregation, leading to specific mesomorphism. However, con-

[a] T. Dutronc, Priv.-Doz. Dr. E. Terazzi, K.-L. Buchwalder, Prof. Dr. C. Piguet
Department of Inorganic, Analytical and Applied Chemistry
University of Geneva, 30 quai E. Ansermet
1211 Geneva 4 (Switzerland)
E-mail: Emmanuel.terazzi@unige.ch
Claude.Piguet@unige.ch

[b] Dr. L. Guénée
Laboratory of Crystallography
University of Geneva, 24 quai E. Ansermet, 1211 Geneva 4 (Switzerland)

[c] Dr. S. Floquet
Institut Lavoisier de Versailles, UMR 8180
University of Versailles Saint-Quentin-en-Yvelines
45 av. des Etats-Unis, 78035 Versailles (France)

Supporting information for this article is available on the WWW under <http://dx.doi.org/10.1002/chem.201503420>.

trary to Trouton's rule for the vaporization of liquids, the entropy changes, ΔS_{tr} , accompanying the melting process that transforms a solid into a liquid or a liquid crystal, or the isotropization process that transforms a liquid crystal into an isotropic liquid, are not constant. They depend on the nature of the material and contribute to the stabilization of the different states of matter.^[13] For instance, the large and variable entropic contributions of the molten flexible chains to the Gibbs free energy have been exploited for the stabilization of the nanosegregated liquid-crystalline phases found in alkylcyanobiphenyls (smectic A mesophase),^[14] bis-alkyloxybenzoylhydrazines (cubic mesophase),^[15] and alkylisothiocyanatibiphenyls (smectic E mesophase).^[16]

Consequently, the square of the Hildebrand solubility parameter, δ^2 , pertinent to the vaporization of liquids, has been replaced by the concept of cohesive free energy density, $CFED = -\Delta G_{tr}^{ref}/V_{mol}$ in liquid crystals, in which $\Delta G_{tr}^{ref} = \Delta H_{tr} - T^{ref}\Delta S_{tr}$ measures the intermolecular cohesion free energy in the solid or in the liquid-crystalline phase estimated at a fixed reference temperature, T^{ref} (ΔH_{tr} and ΔS_{tr} are the enthalpy and entropy changes of the incriminated phase transition, respectively).^[17] Applied to the melting of solid linear alkanes, alkanolic acids, organosilanes, transition metals, or metal oxides, plots of CFED with respect to the melting temperatures systematically display linear correlations, as further illustrated in Figure 1 for methyl-substituted cyanobiphenyls **12-OCB^{i,j}**, which simply melt to give isotropic liquids, despite their amphiphilic character.^[18] To extend the use of the CFED concept into the field of thermotropic liquid crystals, which display successive melting and isotropization transitions, it is necessary to increase the polarity difference ($\Delta\delta = \delta_{tail} - \delta_{head}$) between the antagonist segments originally included in the substituted cyanobiphenyls **12-OCB^{i,j}**. The introduction of an additional *para*-substituted benzoate group gives the *n*-LC^{*i,j*} family (Figure 2), for which an 8–29% increase in $\Delta\delta$ can be computed (Appendix 1 in the Supporting Information). We report herein on the syntheses and structures of the mesogenic extended cyanobiphenyls *n*-LC^{*i,j*}, together with their thermal behavior and liquid-crystalline properties, which are analyzed within the frame of the CFED concept. We believe that its predictive aspects would help in the rational design of the domain of existence of pure liquid-crystalline materials.

Results and Discussion

Standard organic syntheses, relying on Suzuki–Myaura coupling strategies for the preparation of substituted cyanobiphenyls cores,^[17] eventually lead to a complete set of extended cyanobiphenyls *n*-LC^{*i,j*} (Scheme 1; details are given in Appendix 2 in the Supporting Information).

All compounds were characterized by XRD in the crystalline state (Appendix 3 in the Supporting Information). For the non-methylated calamitic molecules *n*-LC^{0,0} (A=B=C=D=H in Scheme 1),^[19] which differ only in the length of the linear aliphatic chains, the crystal structures show long-range polar/apolar segregation and two-dimensional molecular layering (Figure 3). Opposite head-to-head interdigitation stabilized by

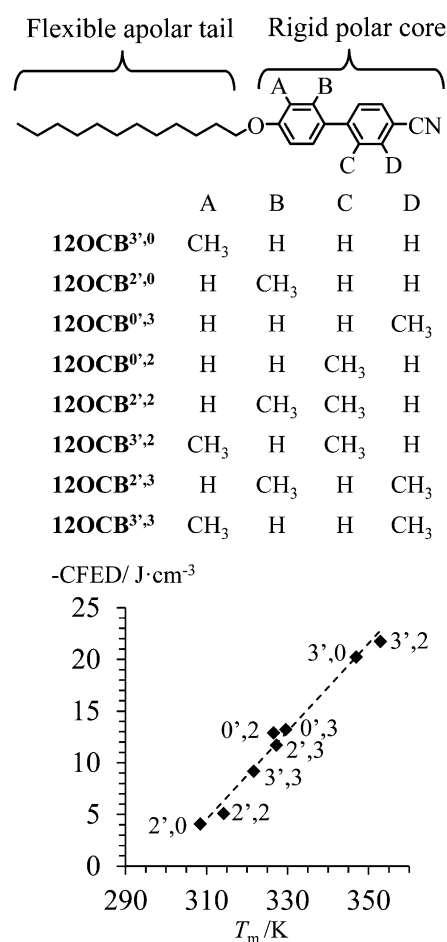


Figure 1. Plot of the CFEDs ($T^{ref} = 298$ K) versus the melting temperatures for the substituted cyanobiphenyls **12-OCB^{i,j}**. Redrawn from ref. [18].

aromatic stacking and hydrogen bonding produces a distance of 9.6(2) Å between the planes defined by the nitrogen atoms of the opposite cyano groups; these planes are tilted by 46.4(6)° with respect to the molecular axis of the rodlike cyanobiphenyl units (Figure 3 and Appendix 4 in the Supporting Information).

Upon methylation of *n*-LC^{*i,j*} ($i \neq 0$ or $j \neq 0$), the intermolecular packing interactions observed in the crystalline state are drastically altered. This perturbation produces variable molecular organizations in the solid state with severely reduced (if any) head-to-head interdigitations of the rigid cyanobiphenyl cores (Appendices 3 and 4 in the Supporting Information). This diversity in intermolecular interactions found in the solid state is mirrored by the formation of various fluidic birefringent textures upon heating solid samples of *n*-LC^{*i,j*} (except for **12-LC^{2',2}**; Figure 4).

This behavior is characteristic of the implementation of specific organizations of the molecules in the liquid-crystalline phases, which could be assigned to smectic and nematic organization by polarized optical microscopy (POM; Figure 5). Temperature-dependent small-angle X-ray scatterings confirmed these assignments because no low-angle diffraction pattern could be detected for the nematic mesophases, where-

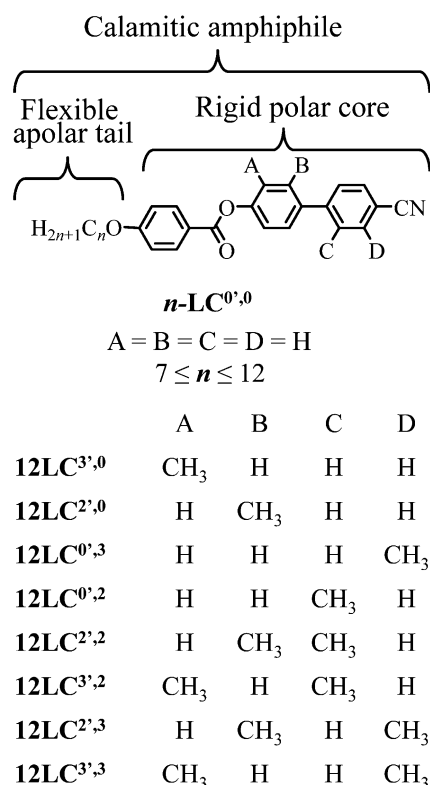
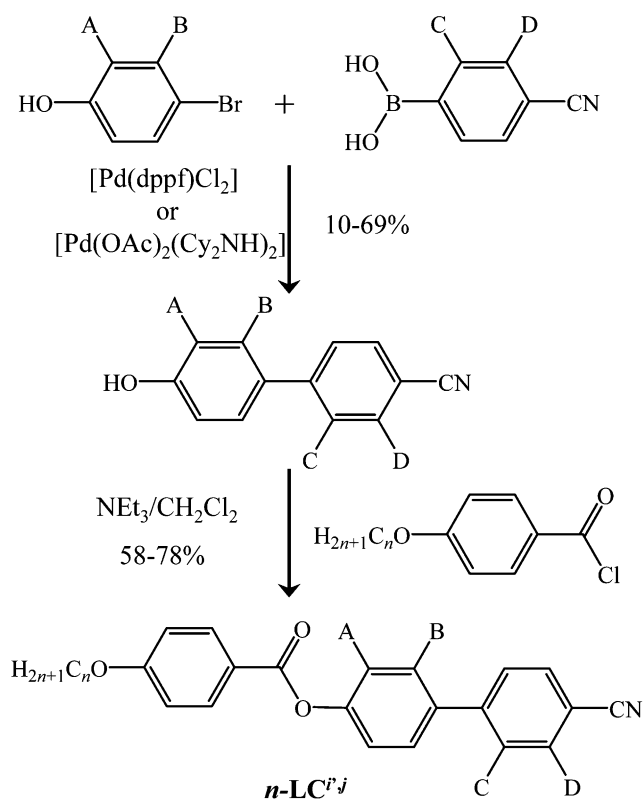


Figure 2. Chemical structures of the substituted cyanobiphenyls $n-LC^{i,j}$ considered herein.



Scheme 1. Syntheses of $n-LC^{i,j}$: dppf = 1,10-bis(diphenylphosphino)ferrocene, Cy₂NH = dicyclohexylamine; A = H or CH₃; B = H or CH₃ (see Figure 2).

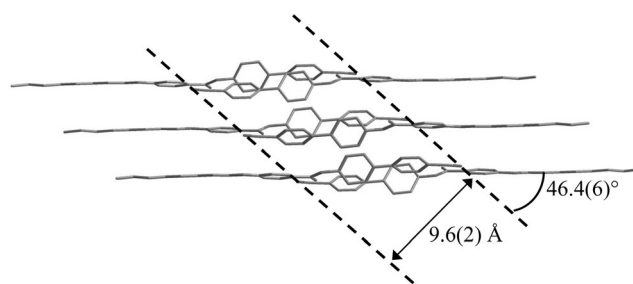


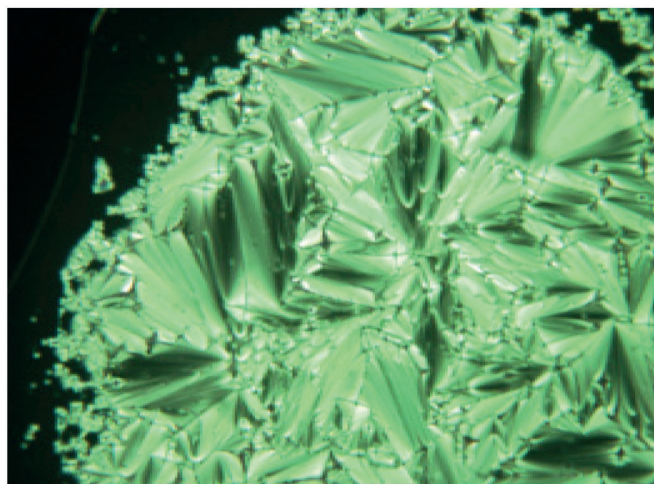
Figure 3. Segregated layer organization in the crystal of $8-LC^{0,0}$, which shows interdigitation between the opposite aromatic cyanobiphenyls and the orientation of the rodlike units in nonsubstituted $n-LC^{0,0}$ compounds.

as a single sharp peak was assigned to the d_{001} reflection in the smectic mesophases (Appendix 5 in the Supporting Information). The calculated interlamellar distances (34.7–41.5 Å) are much shorter than twice the total length estimated for the rodlike molecules in the crystalline state (54–64 Å), which suggests the occurrence of head-to-head interpenetration in the smectic mesophases, probably combined with partial interdigitation of the molten alkyl chains (Table S1 and Figure S1 in the Supporting Information).

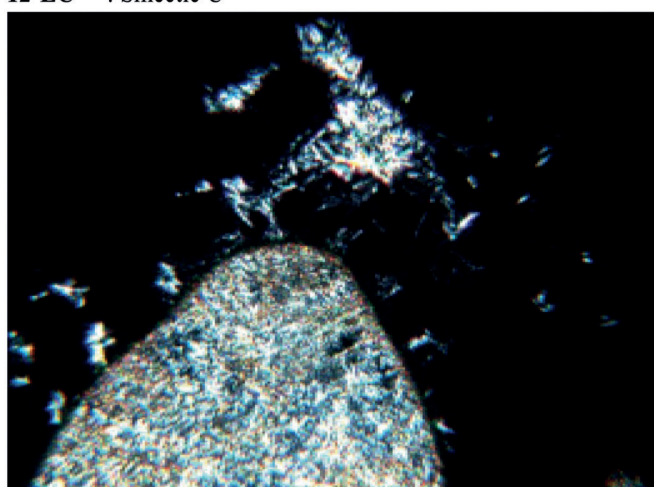
Differential scanning calorimetry (DSC) traces were recorded at 0.5 Kmin⁻¹ for $n-LC^{i,j}$ to minimize deviations from thermodynamic equilibria (Figure 6). Transition enthalpies and entropies for melting (ΔH_m , ΔS_m) and isotropization ($\Delta H_{clearing}$, $\Delta S_{clearing}$) were estimated at the respective transition temperatures by integration of the DSC signals recorded during the heating runs (Table S2 in the Supporting Information). For the nonmethylated calamitic molecules $n-LC^{0,0}$, our observations corroborate those previously reported by Hardouin et al.,^[19] except for some minor differences in the transition temperatures measured by POM, although we refer to the onset of the heat-flow peak monitored by DSC herein (Table S3 in the Supporting Information). Beyond the first-order melting and isotropization transitions, which confirm the thermal behavior established by POM (Figure 5), DSC analyses also reveal some minor solid–solid transitions, cold crystallizations, pretransitional effects, and kinetically enlarged transitions, which are not considered herein because of their negligible enthalpic contributions (Appendix 5 in the Supporting Information).

As previously reported for the nonmesogenic parent molecules **12-OCB^{i,j}**,^[17] the minor perturbation induced by methyl substitution and chain-length increments in $12-LC^{i,j}$ are not expected to drastically alter the minimum intermolecular contact distances in the condensed phases. Consequently,^[20] both melting and isotropization processes obey local linear enthalpy/entropy compensations (Figure 7). The melting temperatures at which solid samples of $n-LC^{i,j}$ transform into liquid crystals cover a narrow range, $343 \leq T_m \leq 376$ K (Figure 5), regardless of 1) the length of the alkyl tail (for $n \geq 7$ methylene rotors) or 2) substitution of the rigid aromatic head. On the contrary, the clearing temperatures at which the liquid-crystalline phases transform into isotropic liquids present a stepwise decrease from $491 \leq T_{clearing} \leq 519$ K for nonsubstituted cyanobiphenyls $n-LC^{0,0}$ (left side of Figure 5) toward

12-LC^{0,0} : Smectic A



12-LC^{0,3} : Smectic C



12-LC^{0,2} : Nematic

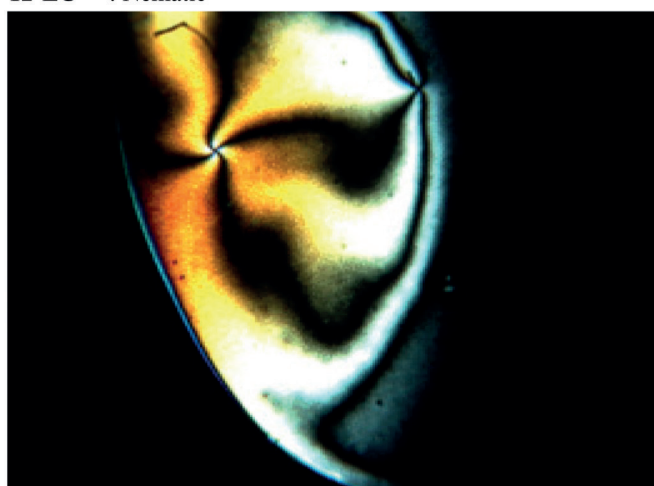


Figure 4. Polarized optical micrographs of 12-LC^{0,0} at 487 K (top, smectic A phase), 12-LC^{0,3} at 358 K (center, smectic C phase), and 12-LC^{0,2} at 416 K (bottom, nematic phase).

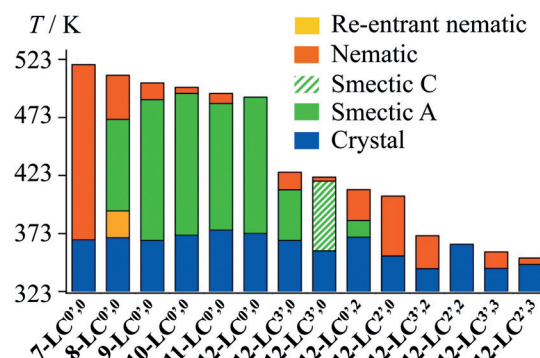


Figure 5. Mesomorphic ranges and observed thermotropic mesophases for $n\text{-LC}^{i,j}$ (scan rate 0.5 K min⁻¹).

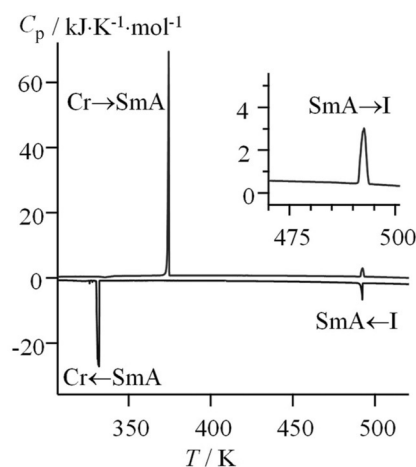


Figure 6. DSC thermograph of 12-LC^{0,0} (scan rate 0.5 K min⁻¹, heating cycle with upward peaks, cooling cycle with downward peaks). Cr = crystal, SmA = smectic A, I = isotropic liquid.

406 ≤ $T_{\text{clearing}} \leq 426$ K for monomethylated cyanobiphenyls 12-LC^{*i,j*} ($i \neq 0$ or $j \neq 0$; central part of Figure 5) and finally toward 352 ≤ $T_{\text{clearing}} \leq 372$ K for dimethylated cyanobiphenyls 12-LC^{*i,j*} ($i \neq 0$ and $j \neq 0$; right side of Figure 5).

Reasonably assuming^[17] that the transition enthalpies and entropies determined at T_m and T_{clearing} , respectively, are not significantly altered when expressed at a common reference temperature, T^{ref} , taken as the average of the observed phase transition processes ($T_m^{\text{ref}} = 360.6$ K and $T_{\text{clearing}}^{\text{ref}} = 443.4$ K), the CFEDs in the solid state, $\text{CFED}_{\text{solid}} = -\Delta G_m / V_{\text{mol}} = -(\Delta H_m - T_m^{\text{ref}} \Delta S_m) / V_{\text{mol}}$ (left part of Figure 8), and in the liquid-crystalline state, $\text{CFED}_{\text{liq-cryst}} = -\Delta G_{\text{clearing}} / V_{\text{mol}} = -(\Delta H_{\text{clearing}} - T_{\text{clearing}}^{\text{ref}} \Delta S) / V_{\text{mol}}$ (right part of Figure 8), can be easily computed with the help of the specific molar volumes, V_{mol} , of $n\text{-LC}^{i,j}$ taken as the Connolly volume estimated in the crystal structures (Appendix 3 in the Supporting Information).^[21] The plots of CFED versus transition temperatures immediately show that the melting and clearing processes are decoupled, each is characterized by its specific linear trend line (Figure 8).

According to the fundamental Gibbs equation of chemical thermodynamics, $S = -(\partial G / \partial T)_p$ ^[22] the slopes of these linear correlations correspond to cohesive entropy densities,

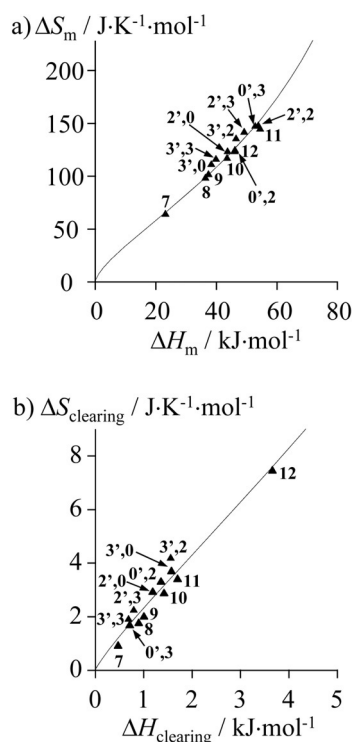


Figure 7. ΔS_{tr} versus ΔH_{tr} plots for a) melting and b) isotropization of $n\text{-LC}^{0,0}$ (n symbol) and $12\text{-LC}^{i,j}$ (monomethylated compounds and dimethylated compounds with i, j symbols), showing local linear H/S compensation. The dashed lines represent reciprocal Hill fits, which obey thermodynamic boundary conditions when $\Delta H_{tr} \rightarrow 0$.^[18]

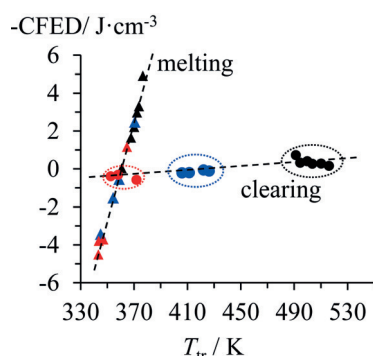


Figure 8. CFEDs versus transition temperatures. $\text{CFED}_{\text{solid}}$ versus melting temperature, T_m (\blacktriangle), and $\text{CFED}_{\text{liq-cryst}}$ versus clearing temperatures, T_{clearing} (\bullet), are displayed for successive phase transitions that occur in non- ($n\text{-LC}^{0,0}$; black), mono- ($12\text{-LC}^{i,j}$ with $i \neq 0$ or $j \neq 0$; blue), and dimethylated ($12\text{-LC}^{i,j}$ with $i \neq 0$ and $j \neq 0$; red).

$\Delta S_{tr}/V_{\text{mol}}$. The steep value of $\Delta S_m/V_{\text{mol}} = 0.253(8) \text{ JK}^{-1} \text{ cm}^{-3}$ observed for the melting of the solids into their liquid-crystalline phases (left part of Figure 8) implies that chemical substitutions of the rigid cyanobiphenyl core in $12\text{-LC}^{i,j}$ have minor effects on the melting temperature. On the contrary, the flat slope of $\Delta S_{\text{clearing}}/V_{\text{mol}} = 0.0054(9) \text{ JK}^{-1} \text{ cm}^{-3}$ found for isotropization of the liquid-crystalline phases into the isotropic liquids (right part of Figure 8) indicates that methylation of the rigid aromatic cores produces large changes in clearing temperatures. Furthermore, we note that successive methylation of the

rigid cores in $12\text{-LC}^{i,j}$ (i.e., zero \rightarrow mono \rightarrow dimethylation) results in three well-separated series that display stepwise decreases in clearing temperatures (Figure 8). The simple but tedious mathematical developments collected in Appendix 6 in the Supporting Information show that 1) the CFED parameter has pressure units ($1 \text{ J cm}^{-3} = 10^6 \text{ Pa}$) and 2) application of the Clapeyron equation^[23] leads to $\text{CFED} = -\lambda dP$, in which λ is the relative molar volume expansion at the transition temperature ($\Delta V_{tr}/V_{\text{mol}}$) of the series of compounds obeying the linear CFED versus T_{tr} correlation. The increment in pressure units for a given member of the series, dP , thus reflects the “chemical changes” or “chemical efforts” required to shift its specific melting temperature toward the reference temperature, T^{ref} , of the family (Figure A6-2 in Appendix 6 in the Supporting Information).

Conclusion

Plots of CFED as a function of the transition temperatures bring quantitative support to chemical intuition^[10] that a thermotropic liquid-crystalline phase is the result of melting of the apolar lipophilic parts of an amphiphilic molecule, while the rigid cores remain partially correlated. For the lipophilic cyanobiphenyls $n\text{-LC}^{i,j}$, a chain length of $n \geq 7$ is sufficient for the demixing of the apolar parts, leading to nanoscale segregation and the formation of thermotropic liquid-crystalline phases for each member of the series (except for $12\text{-LC}^{2,2}$; Figure 5). As expected, substitution (i.e., methylation) of the rigid aromatic core has only a minor influence on the melting temperatures controlled by the entropic contribution of the molten flexible alkyl chains.^[13,16] With the help of the CFED concept, the latter effect can be associated with a cohesive entropy density of $\Delta S_m/V_{\text{mol}} = 0.253(8) \text{ JK}^{-1} \text{ cm}^{-3}$. On the other hand, the clearing temperatures correspond to decorrelations of the rigid aromatic cores, and thus, strongly depend on the methylation of the aromatic part of the cyanobiphenyls in $n\text{-LC}^{i,j}$. Again, the application of the CFED concept provides a quantitative assessment of the effect of peripheral methylation onto the clearing temperature with a cohesive entropy density of $\Delta S_m/V_{\text{mol}} = 0.0054(9) \text{ JK}^{-1} \text{ cm}^{-3}$. In simpler words, methyl substitution of the cyanobiphenyl core can be exploited to tune the clearing temperatures (T_{clearing}), while the melting temperatures (T_m) are essentially invariant (the relative effect can be estimated as $0.253/0.0054 \approx 47$). Finally, the CFED versus T_{tr} correlation highlighted in Figure 8 can be combined with the associated local linear H/S compensations (Figure 7) to give a set of two empirical equations [Eqs. (1) and (2)], which define the domain of existence ($T_{\text{clearing}} - T_m$) of the liquid-crystalline phases.^[17]

$$-\text{CFED} = \frac{\Delta H_{tr} - T_{tr}^{\text{ref}} \Delta S_{tr}}{V_{\text{mol}}} = \alpha T_{tr} + \beta \quad (1)$$

$$\Delta H_{tr} = \gamma \Delta S_{tr} + \varphi \quad (2)$$

For the specific perturbation brought about by successive methylation of the rigid cores of the cyanobiphenyls in $12\text{-LC}^{i,j}$, Figure S2 in the Supporting Information illustrates the

prediction that mesogenic behavior requires a minimal molar volume of $V_{\text{mol}}=200 \text{ cm}^3 \text{ mol}^{-1}$; a much smaller value than those found for non- (489 $\text{cm}^3 \text{ mol}^{-1}$), mono- (503 $\text{cm}^3 \text{ mol}^{-1}$), and dimethylated 12-LC (519 $\text{cm}^3 \text{ mol}^{-1}$).^[24]

Experimental Section

General

The syntheses and characterizations (NMR spectroscopy, ESI-MS, elemental analysis) of the lipophilic cyanobiphenyls *n*-LC^{*f*,*j*} are collected in Appendix 2 in the Supporting Information.

Spectroscopic and analytical measurements

¹H and ¹³C NMR spectra were recorded at 25 °C on a Bruker Avance 400 MHz spectrometer. Chemical shifts are given in ppm with respect to tetramethylsilane (TMS). Pneumatically assisted electrospray (ESI-MS) mass spectra were recorded from 10⁻⁴ M solutions on an Applied Biosystems API 150EX LC/MS system equipped with a Turbo Ionspray source. Elemental analyses were performed by K. L. Buchwalder at the Microchemical Laboratory of the University of Geneva. Thermogravimetric analyses were performed with a thermogravimetric balance by Mettler Toledo Star Systems (under N₂). DSC traces were obtained with a Mettler Toledo DSC1 Star Systems differential scanning calorimeter from 3–5 mg samples (5 and 0.5 °C min⁻¹, under N₂). Conversion: $T(\text{K})=T(^{\circ}\text{C})+273.15$. The characterization of the mesophases and isotropic liquids were performed with a Leitz Orthoplan-Pol polarizing microscope with a Leitz LL 20×/0.40 polarizing objective, and equipped with a Linkam THMS 600 variable-temperature stage. Mathematical analyses were performed by using Igor Pro (WaveMetrics, Inc.) and Excel (Microsoft) software.

X-ray crystallography

Single crystals: Summaries of crystal data, intensity measurements, and structure refinements for compounds *n*-LC^{*f*,*j*} are collected in Tables A3–1 to A3–14 in the Supporting Information. Crystals were mounted on a Kapton loop with protective oil. Cell dimensions and intensities were measured at 180 K on a Supernova (Rigaku) diffractometer with mirror monochromated Cu_{Kα} radiation ($\lambda=1.54184 \text{ \AA}$) and an Atlas charge-coupled device (CCD) camera. Data were corrected for Lorentz and polarization effects and for absorption. The structures were solved by direct methods (SIR97,^[25] SHELXS^[26]) or the charge flipping method (SUPERFLIP);^[27] all other calculations were performed with SHELXL97^[26] and ORTEP^[28] programs.

CCDC-1412272, 1412273, 1412274, 1412275, 1412276, 1412277, 1412278, 1412279, 1412280, 1412281, 1412282, 1412283, 1412285, and 1412285 contain the supplementary crystallographic data for this paper. These data are provided free of charge by The Cambridge Crystallographic Data Centre.

Low-angle powder diffraction: For all samples, the crude powder was filled in Lindemann capillaries of 0.8 mm in diameter. Low-angle powder XRD experiments at various temperatures were performed by using two different diffractometers, depending on the compounds:

1) An Empyrean (PANalytical) diffractometer in capillary mode, with a focusing X-ray mirror for Cu radiation and a PIXcel3D area detec-

tor. Variable temperatures were achieved with a nitrogen cryostreamer (Oxford Cryosystem; available temperatures: 100–500 K).

2) A STOE STADI P transmission powder diffractometer system with a focused monochromatic Cu_{Kα1} beam obtained from a curved Germanium monochromator (Johann-type) and collected on a curved image plate position-sensitive detector (IP-PSD). A calibration with silicon and copper laurate standards, for high- and low-angle domains, respectively, was preliminarily performed. Sample capillaries were placed in the high-temperature attachment for measurements in the range of desired temperatures (from –30 to 240 °C) within 0.05 °C. Periodicities up to 50 Å could be measured.

Acknowledgements

This work was supported through grants from the Swiss National Science Foundation.

Keywords: cyanobiphenyls • liquid crystals • phase transitions • structure elucidation • thermodynamics

- [1] S. Chandrasekhar, *Liquid Crystals*, Cambridge University Press, New York, 1992.
- [2] W. O'Mara, *Liquid Crystal Flat Panel Displays: Manufacturing Science & Technology*, Reinhold Van Nostrand, New York, 1993.
- [3] T. Thiemann, V. Vill, in *Handbook of Liquid Crystals Set* (Eds.: D. Demus, J. Goodby, G. W. Gray, H. W. Spiess, V. Vill), Wiley-VCH, Weinheim, 2008, p. 87.
- [4] a) L. Onsager, *Ann. N. Y. Acad. Sci.* 1949, 51, 627–659; b) G. J. Vroege, H. N. W. Lekkerkerker, *Rep. Prog. Phys.* 1992, 55, 1241–1309.
- [5] a) W. Maier, A. Saupe, *Z. Naturforsch. A* 1959, 13, 564–570; b) W. Maier, A. Saupe, *Z. Naturforsch. A* 1959, 14, 882–900; c) W. Maier, A. Saupe, *Z. Naturforsch. A* 1960, 15, 287–292; d) A. Saupe, *Angew. Chem. Int. Ed. Engl.* 1968, 7, 97–118; *Angew. Chem.* 1968, 80, 99–115; e) G. R. Luckhurst, C. Zannoni, *Nature* 1977, 267, 412–414.
- [6] a) C. Tschierske, *Ann. Rep. Prog. Chem. Ser. C* 2001, 97, 191–267; b) C. Tschierske, *Top. Curr. Chem.* 2011, 318, 1–108.
- [7] F. T. Trouton, *Philos. Mag.* 1884, 18, 54–57.
- [8] a) J. H. Hildebrand, R. L. Scott, *The Solubility of Nonelectrolytes*, 3rd Ed., Reinhold Pub Group, New York, 1950; b) C. M. Hansen, *Solubility Parameters: A User's Handbook*, 2nd ed., CRC Press, Boca Raton, 2007, Chapter 1.
- [9] a) E. Bialecka-Florjanczyk, *J. Phys. Chem. B* 2006, 110, 2582–2592; b) M. Yoneya, K. Araya, E. Nishikawa, H. Yokoyama, *J. Phys. Chem. B* 2004, 108, 8099–8101; c) M. Yoneya, *Chem. Rec.* 2011, 11, 66–76.
- [10] a) A. Skoulios, *Advances in Liquid Crystals* (Ed.: G. Brown), Academic Press, New York, 1975, part 1, p. 169; b) D. Guillon, A. Skoulios, *J. Phys.* 1976, 37, 797–800; c) A. Skoulios, D. Guillon, *Mol. Cryst. Liq. Cryst.* 1988, 165, 317–332. For a comprehensive review, see C. Tschierske, *Angew. Chem. Int. Ed.* 2013, 52, 8828–8878; *Angew. Chem.* 2013, 125, 8992–9047.
- [11] a) C. Tschierske, *J. Mater. Chem.* 1998, 8, 1485–1508; b) A. Pegenau, T. Hegmann, C. Tschierske, S. Diele, *Chem. Eur. J.* 1999, 5, 1643–1660; c) C. Tschierske, *J. Mater. Chem.* 2001, 11, 2647–2671.
- [12] C. Tschierske in *Handbook of Liquid Crystals, Vol. 5*, 2nd ed. (Eds.: J. W. Goodby, P. J. Collings, T. Kato, C. Tschierske, H. F. Gleeson, P. Raynes), Wiley-VCH, Weinheim, 2014, pp. 1–43.
- [13] K. Saito, T. Miyazawa, A. Fujiwara, M. Hishida, H. Saitoh, M. Massalska-Arodz, Y. Yamamura, *J. Chem. Phys.* 2013, 139, 114902.
- [14] Y. Yamaoka, Y. Taniguchi, S. Yasuzuka, Y. Yamamura, K. Saito, *J. Chem. Phys.* 2011, 135, 044705.
- [15] Y. Nakazawa, Y. Yamamura, S. Kutsumizu, K. Saito, *J. Phys. Soc. Jpn.* 2012, 81, 094601.
- [16] T. Miyazawa, Y. Yamamura, M. Hishida, S. Nagatomo, M. Massalska-Arodz, K. Saito, *J. Phys. Chem. B* 2013, 117, 8293–8299.

- [17] T. Dutronc, E. Terazzi, L. Guéneé, K.-L. Buchwalder, A. Spoerri, D. Emery, J. Mareda, S. Floquet, C. Piguet, *Chem. Eur. J.* **2013**, *19*, 8447–8456.
- [18] T. Dutronc, E. Terazzi, C. Piguet, *RSC Adv.* **2014**, *4*, 15740–15748.
- [19] F. Hardouin, A. M. Levelut, N. H. Tinh, G. Sigaud, *Mol. Cryst. Liq. Cryst.* **1979**, *56*, 35–41.
- [20] a) D. M. Ford, *J. Am. Chem. Soc.* **2005**, *127*, 16167–16170; b) C. Piguet, *Dalton Trans.* **2011**, *40*, 8059–8071.
- [21] The molecular volumes are taken as the Connolly volumes, which are obtained by building the Connolly surface around the molecular structures of complexes observed in the crystal structures with a probe radius of 1.4 Å to model water solvent molecules (M. L. Connolly, *Science* **1983**, *221*, 709–713. M. L. Connolly, *J. Appl. Crystallogr.* **1983**, *16*, 548–558).
- [22] P. W. Atkins, J. de Paula, *Physical Chemistry*, 9th ed., W. H. Freeman and Company, New York, **2010**, p.124.
- [23] P. W. Atkins, J. de Paula, *Physical Chemistry*, 9th ed., W. H. Freeman and Company, New York, **2010**, p.147.
- [24] The very limited range of molecular volumes spanned by the experimental data collected for molecules **12-LC^{ij}** in this work results in relatively large uncertainties that affect the coefficients α , β , γ , and φ of the linear correlations depicted in Equations (1) and (2). Hence, only trend lines for the phase boundaries are accessible in Figure S2 in the Supporting Information.
- [25] A. Altomare, M. C. Burla, M. Camalli, G. Cascarano, C. Giacovazzo, A. Guagliardi, G. Moliterni, G. Polidori, R. Spagna, *J. Appl. Crystallogr.* **1999**, *32*, 115.
- [26] G. M. Sheldrick, SHELXL97 Program for the Solution and Refinement of Crystal Structures, University of Göttingen, Germany, **1997**.
- [27] L. Palatinus, G. Chapuis, *J. Appl. Crystallogr.* **2007**, *40*, 786.
- [28] ORTEP3, L. J. Farrugia, *J. Appl. Crystallogr.* **1997**, *30*, 565.

Received: August 28, 2015

Published online on December 14, 2015